DOI: 10.26599/FSHW.2026.9250960

Contents lists available at SciOpen

Food Science and Human Wellness

journal homepage: https://www.sciopen.com/journal/2097-0765

China Food Publishing Co.

Thermostability improvement of quinone-dependent dehydrogenase by computation-aided phylogeny-oriented engineering

Bin Ma[a], Juan Shen[a], Jiafeng Niu[a], Hao Zhu[a], Jiali Liu[a], Huibing Chi[a], Zhaoxin Lu[a], Fengxia Lu[a,*], Ping Zhu[a,*]

[a]*College of Food Science and Technology, Nanjing Agricultural University, Nanjing 210095, China*

ABSTRACT: Deoxynivalenol (DON), a mycotoxin with global distribution, has caused serious economic losses and poses food and feed safety issues. Recently, a quinone-dependent dehydrogenase (DADH) was identified to degrade DON into the less toxic 3-keto-DON by oxidation of the critical toxic hydroxyl group, which was then reduced by aldo-keto reductase AKR13B3 into the relatively non-toxic 3-*epi*-DON. Nevertheless, the poor thermostability of DADH limits its practical application. Here, a combinatorial mutant M3 with significantly improved thermostability was screened using computation-aided design combining ancestral sequence reconstruction and structural analysis. The mutants M3 exhibited high thermostability with an 8.93-fold longer half-life at 55℃ than that of wild-type. Moreover, structural analyses and molecular dynamics simulations revealed that the reduced flexibility, enhanced structural rigidity, favorable electrostatic potential, and increased number of hydrogen bonds in mutant M3 were the primary factors underlying its improved thermostability. This work provides a facile and efficient strategy to improving the thermostability of DON detoxification enzymes for agricultural and food industry applications.

Keywords: dehydrogenase, deoxynivalenol, thermostability, ancestral sequence reconstruction, molecular dynamics simulation

1. Introduction

The deoxynivalenol (DON) is a secondary metabolite produced by *Fusarium* species serious, seriously threatens food and feed safety (Schmied et al., 2023; Sumarah, 2022). DON contamination poses a global health threat due to its demonstrated immunotoxic, cytotoxic, and genotoxic effects, presenting significant risks to humans and animals through multiple exposure routes (Deng et al., 2023; Zhang et al., 2024). These factors emphasize that the necessity of developing effective approaches to degrade DON is necessary in agricultural and food processing systems (Tu et al., 2023). Some studies have demonstrated the limitations of physical and chemical methods for degrading DON in terms of inefficiency, insecurity and susceptibility to nutrient loss (Fang et al., 2022; Guo et al., 2024). Utilizing microorganisms and enzymes for detoxification is a green and efficient way to reduce DON contamination, which can degrade DON to low-/non-toxic products (Yao et al., 2024). The main toxic groups of enzyme-catalyzed DON are C12/C13, C9=C10, and C3-OH (Tian

***Corresponding author**
Fengxia Lu, lufengxia@njau.edu.cn;
Ping Zhu, E-mail: pingzhu@njau.edu.cn

Received 25 August 2025
Received in revised from 22 September 2025
Accepted 13 October 2025

et al., 2022), comprising oxidation (He et al., 2020), acetylation (Khatibi et al., 2011), glycosylation (Tian et al., 2016), glutathionylation (Yang et al., 2024) and isomerization (Carere et al., 2018b).

The C3 hydroxyl group is one of the major toxic groups in DON. Currently, some microorganisms were able to efficiently convert DON to the less-toxic 3-keto-deoxynivalenol (3-keto-DON) and/or the non-toxic 3-*epi*-deoxynivalenol (3-*epi*-DON), such as *Devosia* strain D6-9, *Devosia* insulae A16, *Nocardioides* sp. ZHH-013, and *Sphingomonas* S3-4 (He et al., 2020; He et al., 2017; Wang et al., 2019; Zhang et al., 2021). There were some enzymes, including DepA, QDDH, AKR18A1, DDH, SDH that could convert DON to 3-keto-DON (Carere et al., 2018a; He et al., 2020; He et al., 2017; Li et al., 2023; Qin et al., 2022). We identified two DON-degrading enzymes from *Devosia* strain A6-243, named DADH and AKR13B3 (Niu et al., 2024). DADH could convert DON to less-toxic 3-keto-DON, but DADH had poor catalytic activity and thermostability. In prior research, the mutant L110V/V429A (named DADH-V2) with improved catalytic activity and substrate specificity had been successfully obtained by active pocket remodeling (Ma et al., 2024). Nevertheless, the deficiency in thermal stability greatly limited its potential for practical applications. The engineered detoxification enzyme M10 was reported to be able to degrade deoxynivalenol, retaining 77% and 19% of its activity at 45℃ and 50℃, respectively (Yang et al., 2024). To satisfy industrial applications, enhancing the thermal stability of DON detoxifying enzymes is essential. Consequently, the focus of this study is to enhance the thermal stability of DADH-V2, a critical improvement for its effectiveness in detoxifying DON within food and feed production systems.

With the rapid development in the fields of bioinformatics and computational biology, enzyme ancestral sequence reconstructions (ASRs) is an advantageous strategy used to gain information about gene evolution, and has emerged as a laudable and effective method to improve enzyme thermal stability (Gumulya et al., 2018; Wang et al., 2024). During the process of enzyme evolution, the need to adapt to environmental changes, especially extreme conditions, has spurred the emergence of advantageous characteristics (Chen et al., 2022). One such characteristic is an improvement in thermal stability, enabling enzymes to remain functional at elevated temperatures (Yang et al., 2023). Consequently, thermophilic ancestral enzymes were probably found in this evolutionary landscape. Numerous ancestral enzymes are present in multiple branches across the evolutionary landscape (Schupfner et al., 2020). Notably, given branch lengths, ASRs are produced within related groups and are different from consensus proteins (Randall et al., 2016). Additionally, it is vital to discover the relationship between ASRs and ancestral enzymes, as potentially beneficial residues recognized through ASRs might help to enhance the thermal stability of specific enzymes (Spence et al., 2021). Ancestral enzymes originating from ASRs also exhibited enhanced activity, improved solubility and altered promiscuity (Thomson et al., 2022). By comparing the sequence, structure, and function of progeny and ancestral intermediates, ASRs can recognize functionally significant substitutions from the enzyme's evolutionary history, thereby contributing to the construction of promising mutants for industrial applications (Yosephine et al., 2017). The ASRs studies had successfully enhanced the thermal stability of β-xylosidases,

D-amino acid oxidase, and nitrilase, further proving its potential in improving the thermal stability of enzymes (Wang et al., 2023).

In this study, the previously studied optimal variant, DADH-V2, was selected as our starting strain. Then, we leveraged computation-aided design combining ancestral sequence reconstruction and structural analysis to enhance its thermostability. A mutant featuring improved thermal stability was procured via the techniques of site-directed saturation mutagenesis and combinatorial mutagenesis. Ultimately, the mechanism underlying the improved thermal stability of the optimal mutant was clarified by structure prediction, molecular docking, and molecular dynamics (MD) simulations. The present work showed how computationally-aided phylogeny-oriented engineering could effectively enhance the thermal stability of detoxifying enzymes. Moreover, it offered novel strategies and perspectives for improving the thermal stability of vomitoxin detoxification enzymes.

2. Materials and methods

2.1. Bacterial, strains and chemicals

The *Escherichia coli* (*E. coli*) BL21 (DE3) was used as the host for protein expression. The DADH-V2 genes were cloned into the expression vector pET-28a (+). The 2 × Proofast Max Master Mix and recombination biochemical regent test kits were purchased from ATG Biotechnology Co., Ltd (Nanjing, China). All primers were purchased from GenScript (Nanjing, China). DON and 3-keto-DON were purchased from TripleBond (Guelph, ON, Canada). Pyrroloquinoline quinone (PQQ)and chemical reagents were purchased from Aladdin (Shanghai, China).

2.2. Computation-aided design of DADH-V2

The amino acid sequence of DADH-V2 was submitted to the National Center for Biotechnology Information database (NCBI, https://www.ncbi.nlm.nih.gov/). The ancestral sequence of DADH-V2 was reconstructed by the FireProt-ASR online tool (https://loschmidt.chemi.muni.cz/fireprotasr/), and the evolutionary conservation of amino acids was evaluated based on multiple sequence alignment obtained from MEGA11 (Tamura et al., 2021). The maximum likelihood approach implemented in MEGA11 was utilized to construct a phylogenetic tree, and bootstrap analysis with 1,000 repetitions was performed to evaluate the reliability of the tree. The CUPSAT (https://cupsat.brenda-enzymes.org/) was then used to choose candidate sites with Gibbs free energy change ($\Delta\Delta G$) > 1 kcal/mol and > 1/3 stable mutagenesis in the profitable region were chosen for further testing.

2.3. Construction of the DADH-V2 mutant library

A site-directed mutagenesis library was constructed using the PCR-based method (Niu et al., 2023), and the primers required for mutagenesis were listed in Table S1. Briefly, the plasmid pET 28a-DADH-V2 was used as the template. After completing the PCR cycle, and then the PCR cycle product was digested with DpnI. Finally, the recombinant plasmids were used to transform transformed into *E. coli* BL21 (DE3) for

screening of mutants with enhanced thermal stability. Combinatorial mutants were obtained using positive mutant with significantly improved thermal stability as templates.

2.4. Protein expression and purification

E. coli strains were cultured in LB medium containing 50 μg/mL kanamycin at 37℃ for 12 h. The culture was moved into fresh LB medium and cultured at 37℃. After OD_{600} reached 0.6-0.8, the isopropyl β-D-1thiogalactopyranoside (at a concentration of 100 μg/mL) was added, and incubated for 16-20 h at 16℃. Cells were collected and lysed by sonication, and the supernatant was transferred to a Ni-NTA resin affinity column (GenScript, Nanjing, China). The column was eluted with a buffer containing 50 mM imidazole, and elution of the target protein was accomplished by using a buffer containing 500 mM imidazole.

2.5. Enzyme activity assay

Enzyme activity assays were performed according to the previous method (Yang et al., 2022). Briefly, the reaction mixtures containing 10 μg enzyme, 50 mM Tris-HCl buffer (pH 7.5), 1 mM Ca^{2+}, 0.1 mM PQQ, 0.25 mM 2,6-dichloropheno-lindophenol (DCPIP), 0.05 mM phenazine methosulfate (PMS), 0.1 mM DON were utilized. One unit of enzyme activity was defined as the amount of enzyme reduction one μmol DCIP per minute.

2.6. Analysis of the thermostability of DADH-V2 and its mutant

The half-life ($t_{1/2}$) and melting temperature (T_m) were used to assess the thermal stability of AKR-V3 and its variants. For the T_m of AKR-V3 and its mutants to be determined, thermal shift assays were conducted by the Protein Thermal Shift Dye kit (Thermo-Fisher Scientific, Waltham, MA, USA). The samples were diluted to a final protein concentration of 1.5 mg/mL and the dye was diluted to 16 × as a working solution. Samples were subsequently subjected to thermal denaturation in a StepOne real-time PCR with a temperature gradient from 25 to 99℃. T_m was measured as the midpoint of the fluorescence increase.

To calculate $t_{1/2}$, the enzyme was incubated at 55℃ and the activity was measured at regular intervals. Enzyme buffer was incubated at 55℃ for different times and then immediately put on ice. The initial enzyme activity was 100%, and the activity of the samples taken out at different incubation times was the residual activity. The $t_{1/2}$ was calculated by the equation $t_{1/2}= \ln 2/k_d$, the decay constant (k_d) was determined by the first-order linear regression using the formula $\ln A = k_d \times t$, where A was residual activity, t was incubation time.

2.7. Determination of enzyme properties

The optimal pH of the DADH-V2 and variants was investigated with a pH range of 5-9. The optimal reaction temperature of the DADH-V2 and variants was conducted from 30-60℃. The highest activity was taken as 100%, and the enzyme activity at other temperatures was the relative activity at that temperature. The kinetic parameters of DADH-V2 and its variants were evaluated by determining the reaction rates of different concentrations of the substrate DON from 0.1 to 10 mM. Nonlinear fitting was performed using GraphPad

Prism 8.0 software (GraphPad Software, Inc., San Diego, CA) to derive the Michaelis-Menten equation, followed by the kinetic correlation data were obtained (Nie et al., 2018).

2.8. Structure prediction and molecular dynamics simulations

The three-dimensional structures of DADH-V2 and variants were predicted by AlphaFold 3 (https://alphafoldserver.com/). The protein structures were visualized and analyzed via PyMOL. The molecular docking analysis was performed using AutoDock Vina 1.2.3. MD simulations were performed using AMBER 20 software. The AMBER ff14SB force field was utilized for MD simulations. The proteins were solvated in a TIP3P water box for each simulation system and extended 10 Å from the protein surface. The charges of the system were neutralized using Na^+ or Cl^-. The system was subjected to energy minimization by the steepest descent method. Subsequently, the system temperature was carried out at 330 K for 50 ns. The atomic trajectories were analyzed to generate root-mean-square deviation (RMSD), root-mean-square fluctuation (RMSF), solvent-accessible surface area (SASA), and radius of gyration (Rg).

3. Results and discussion

3.1. Mutation design based on ASRs and computation-aided strategy of DADH-V2 (WT)

Researchers believed that extreme thermophilic ancestral enzymes were possible in the evolution of enzymes (Brennan et al., 2024). However, they might also be at risk of extinction during evolution. Luckily, people could use ancestral enzyme reconstruction techniques to infer the amino acid sequences of all ancestral enzymes in the evolutionary landscape, thus gaining insights into the primary structure (amino acid sequence) of these ancestral enzymes. In this study, to create dehydrogenases with enhanced thermal stability, we employed the ASRs technique, using WT as the initial enzyme template. Subsequently, amino acid sequences with 30%-90% homology to the target protein were obtained from the NCBI database. After removing redundant and over-short sequences, the obtained dehydrogenase was constructed into a phylogenetic tree utilizing the ancestral sequence reconstruction tool FireProt-ASR (Figure 1A and Figure S1). In addition, WT was subjected to multiple sequence alignment with these 150 ancestral sequences obtained via ASRs to assess nonconserved residues that might impact the thermal stability of WT (Figure S1). Finally, 108 amino acid residues were identified as potential stabilizing mutation sites. To eliminate residues that interfere with catalytic activity by mutation, residues within 5 Å of the active center were removed (Figure 1B). One residue (F177) was excluded due to its location within 5 Å of the active site, while the remaining 107 residues were selected for further analysis (Figure S2). To further construct small and high-quality mutant libraries, screening was performed using CUPSAT to assess the change in stability at each candidate site according to the variation in free energy ($\Delta\Delta G$) between wild-type and variants (Figure 1A). By preliminary calculations, 29 hotspots were larger than the threshold ($\Delta\Delta G$ value > 1 kcal/mol and > 1/3 of the amino acids residues in the favored region) and thus were selected for further experimental validation (Figure 1C and Figure S2).

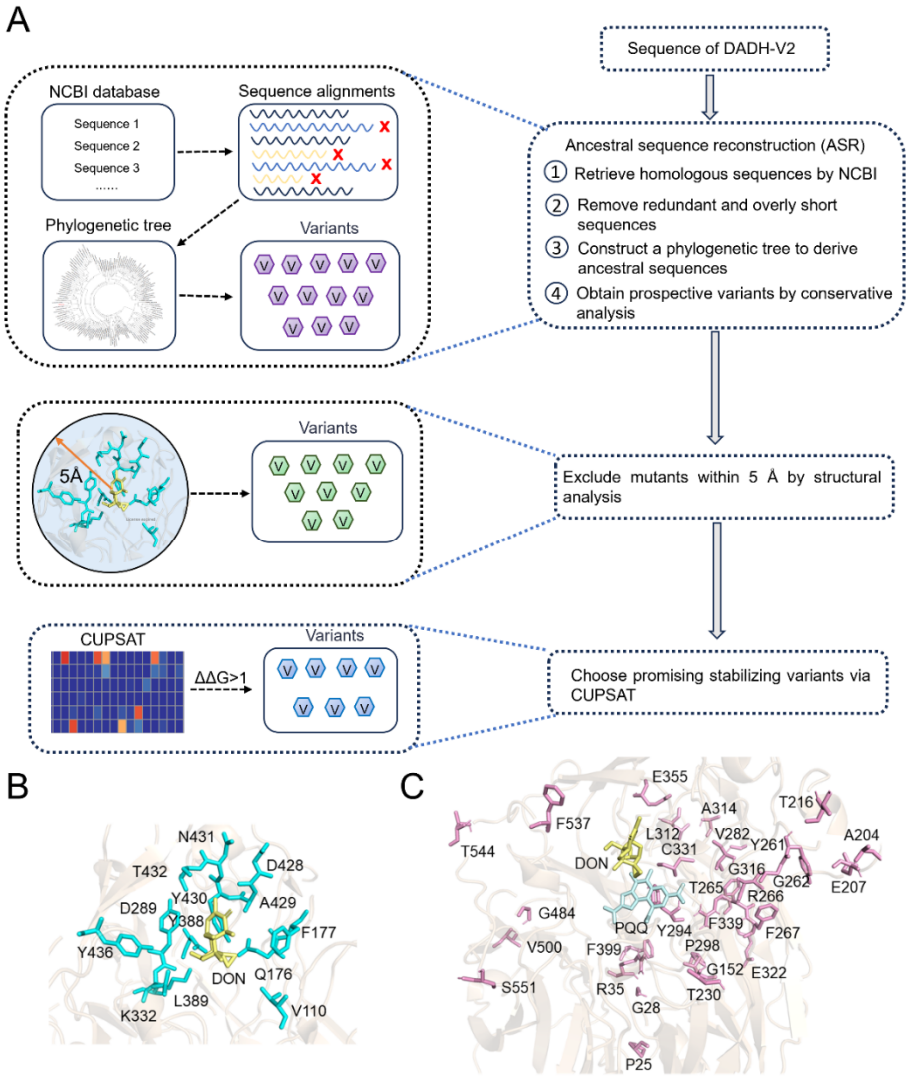

Figure 1. (A) The scheme for engineering the thermal stability of DADH-V2 by using ancestral sequence reconstruction, structural analysis and virtual saturation mutagenesis. (B) Residues within 5 Å from the active center. Residues were presented in cyan sticks. (C) Locations of the mutations sites in 3D structure of DADH-V2. Residues were presented in pink sticks.

3.2. Site-directed mutagenesis to improve the thermostability of WT

Mutants demonstrating enhanced thermostability were meticulously selected according to their residual activity and relative activity metrics. As shown in Figure 2, the residual and relative activities of 29 mutants were constructed in this experiment. 5 mutants (F537M, Y294F, E355Q, E207P and S551P) had higher relative activity (> 80%) (Figure 2A). Of these mutants, F537M, Y294F, E207P and S551P exhibited improved thermal stability, with residual activities of 64.0%, 55.2%, 50.2% and 52.4%, respectively, after 4 min of treatment at 55℃ (Figure 2B). Due to the lower residual activity of mutant E355Q (31.3%), thus not considered as a potential mutational hotspot. Consequently, 4 single-point mutants with improved thermal stability and activity were obtained (Figure 3A). Given the potential synergy among mutations, a randomized combination of 4 mutations was conducted to generate 6 double-site mutants. Among the set of combinatorial mutants, the double-site mutant, F537M/E207P (M1), presented the highest thermostability with residual activity (51.1%) and relative activity (87.4%) after treatment at 55℃ for 12 min (Figure 3B). Based on the

results achieved, mutant M1 was selected as the template for the subsequent round of mutagenesis aimed at enhancing thermostability, resulting in 2 triple-site mutants. The results showed that the mutant F537M/E207P/S551 (M2) exhibited higher residual activity (59.5%) than M1, and there was no significant decrease in relative activity (85.2%). Subsequently, the mutant M2 was chosen as the mutagenesis template for further increase in thermostability, and 1 quadruple-site mutant was constructed. As shown in Figure 3B, the relative activity (93.0%) and residual activity (64.2%) of the mutant F537M/E207P/S551P/Y294F (M3) were both enhanced compared with that of M2. It had been reported that mutant V29P showed almost no degradation of DON after incubation at 45℃, while mutant M10 retained 77% of its residual activity, with only 19% of activity at 50℃ (Yang et al., 2024). As a result, M3 displayed excellent thermostability while retaining high activity.

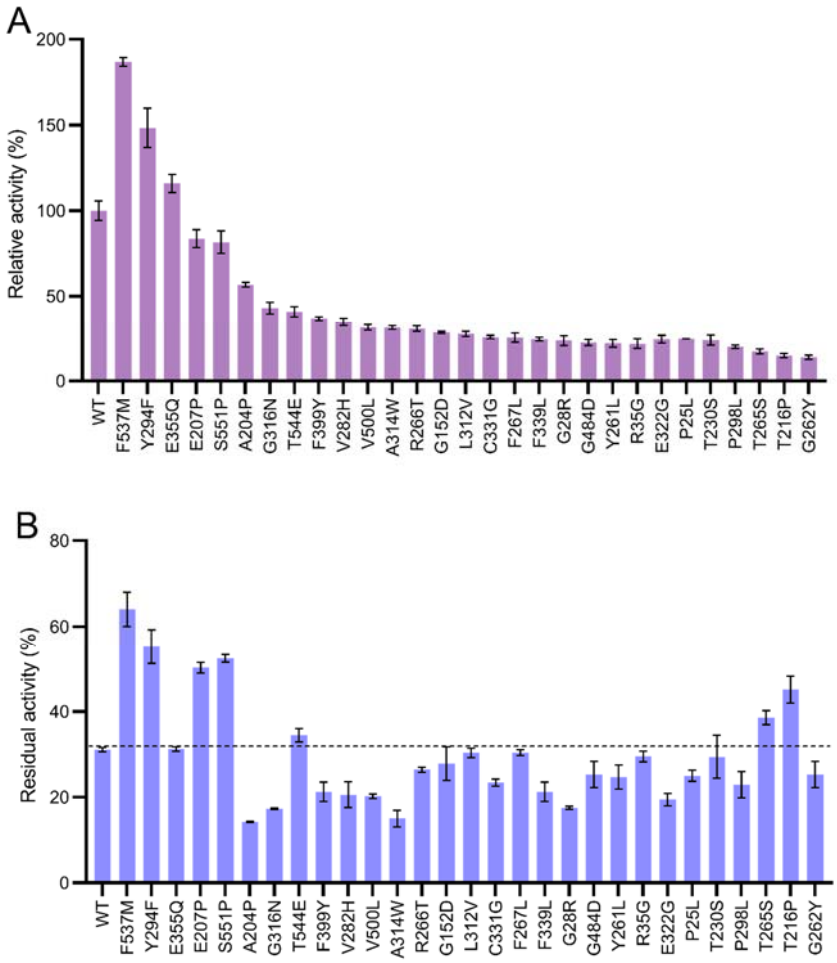

Figure 2. Construction of mutant libraries. (A) Construction of mutants and determination of relative enzyme activity. (B) Construction of mutants and determination of residual enzyme activity at 55℃ for 4 min.

Moreover, the improved thermostability was further confirmed by studying T_m and $t_{1/2}$ of the mutants. The $t_{1/2}$ values of mutants F537M, E207P, Y294F and S551P at 55℃ were 6.31, 4.56, 5.87 and 5.35 min (Figure 3C), respectively, representing 3.05-, 2.20-, 2.84- and 2.58-fold improvements compared to that of WT (2.07 min). Furthermore, the $t_{1/2}$ of M1 at 55℃ increased to 11.1 min, which was longer than that of WT, representing a synergistic effect produced by the combination of the two single-point mutants. Moreover, the mutations of Y294F and S551P were sequentially assembled into M1, and the resulting mutants, namely, M2

and M3, enhanced the $t_{1/2}$ values to 15.6 and 18.5 min, respectively, which was 7.54- and 8.93-fold higher compared to WT. Compared to the WT, the T_m values of all four single-point mutants were also increased (Figure 3D). The improvement was also presented in T_m values, with a 4.6℃ increase for M3 (66.1℃), compared with that for WT (61.5℃). These results indicated that there was a synergistic effect between these residues, which could effectively improve the thermostability (Chen et al., 2023). Thus, we succeeded in obtaining a four-point mutant M3 with a significant improvement in thermostability.

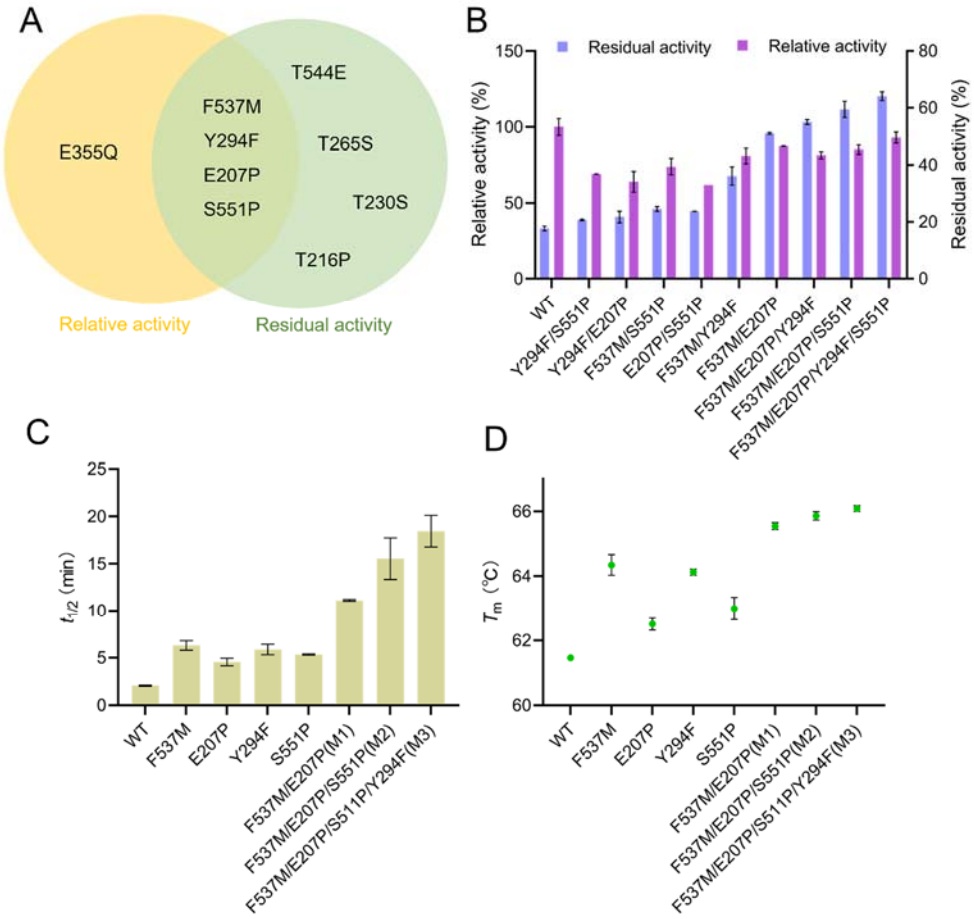

Figure 3. Construction of combinatorial mutant libraries and thermostability of mutants. (A) Yellow circles represented mutants with increased relative activity. Green circles represented mutants with increased residual activity. Overlapping regions were mutants with increased in both relative activity and residual activity. (B) Residual activity of the combinatorial mutants. (C) Half-life ($t_{1/2}$) of WT and mutants. The detection of $t_{1/2}$ was accomplished by assaying the residual activity of WT and mutants after incubation at 55℃ for different times. (D) T_m value of WT and mutants.

3.3. Enzymatic characterization of WT and mutant M3

To further explore the potential of the best mutant as a biocatalyst for industrial applications, we further characterized its enzymatic properties. The optimal reaction temperature for both mutant M3 and WT was 40℃ (Figure 4A). Additionally, WT and M3 were heated at 55, 60, and 65℃, respectively. The residual activity of WT decreased to 15.9% after 15 min of treatment at 55℃ (Figure 4B), to 9.21% after 12 min of treatment at 60℃ (Figure 4C), to 8.28% after 6 min of treatment at 65℃ (Figure 4D). Compared with the WT, the residue activity of M3 was 55.9% after 15 min of treatment at 55℃ (Figure 4B), 33.7% after 12 min of treatment at 60℃ (Figure 4C), 35.1% after 6 min of treatment at 65℃ (Figure 4D), respectively. The optimum reaction pH was assayed at pH 5-10. As depicted in Figure 4E, mutant M3 presented an optimum pH of 7.5,

which was the same as that of WT. As we know, the enzyme's optimal pH is affected by several factors, including the pKa value of the active site residues, enzyme substrate binding, and enzyme surface charge (Hasan et al., 2024). Understanding the mechanism of mutation-induced pH changes requires further experimental validation, such as clarification of the ionization state and pKa value of each residue (Cai et al., 2018). Furthermore, the kinetic parameters of WT and M3 were studied under optimal conditions. The results of the study showed that none of the k_{cat} and K_m values of the M3 were not greatly altered compared to WT (Table S1). This breaks the equilibrium where stability and activity might influence each other (Truongvan et al., 2016). Thus, we obtained the mutant M3 with greatly improved thermal stability and no significant reduction in activity, which gives it potential for practical applications.

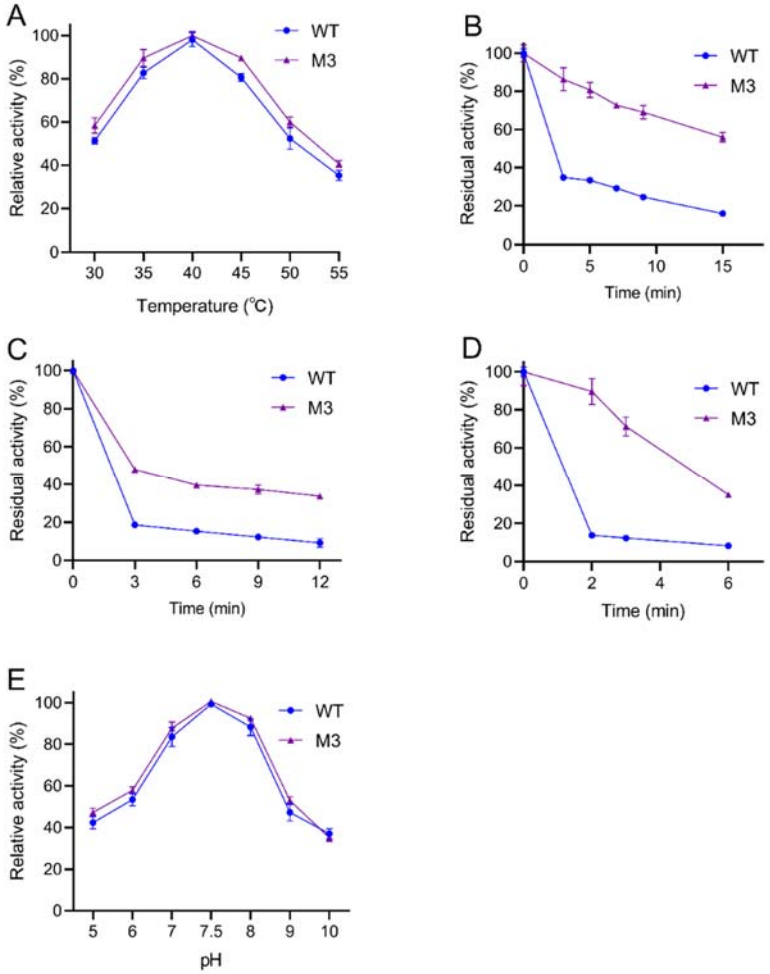

Figure 4. Enzymatic properties of WT and mutant M3. (A) Optimal temperature of WT and M3. Thermostability of WT and M3 at 55℃ (B), 60℃ (C), 65℃ (D). Optimum pH of WT and M3 (E).

3.4. Insights into the origin of enhanced thermostability of mutant M3

Generally, the thermostability of proteins was considered to be positively correlated with hydrophobicity and negatively correlated with flexibility. As shown in Figure S3, the hydrophobicity and flexibility of WT and M3 were investigated. The E207 and Y294 sites were replaced with P207 and F294, respectively, resulting in increased hydrophobicity of the 202-210 and 289-297 loops (Figure S3A). Additionally, compared to the wild-type, the substitutions at positions Y294 and F537 resulted in reduced flexibility of the

289-297 and 532-540 loops (Figure S3B). These results suggested that the improved thermostability of M3 might be related to structurally enhanced hydrophobicity and reduced flexibility.

To gain a deeper understanding of the molecular mechanisms that enhance the thermal stability of M3. We obtained a structural model of DADH-V2/PQQ using the AlphaFold server and then docked the substrate DON to the pocket via AutoDock Vina 1.2.3 (Figure 5A). Mutations-induced conformational alterations exhibited an intrinsic correlation with the enhanced stability of enzymes. As seen from Figure 5B and C, all four mutation sites were replaced by hydrophobic amino acids. For the Y294F mutation, phenylalanine (F, with a benzene ring side chain) replaces tyrosine (Y) at position 294, potentially promoting the formation of a robust hydrophobic core (Figure S4). These hydrophobic residues on the surface and inside of the enzyme play a critical role in the structural stability of the enzyme (zhang et al., 2024), which was consistent with previous results (Figure S3A). Increasing the thermostability of the enzyme by introducing proline was a popular strategy due to the fact that proline had a low conformational freedom pyrrolidine ring (Wu et al., 2023). Consequently, residue E207P and S551P enhanced the local rigidity, resulting in the increase of the enzyme's thermal stability.

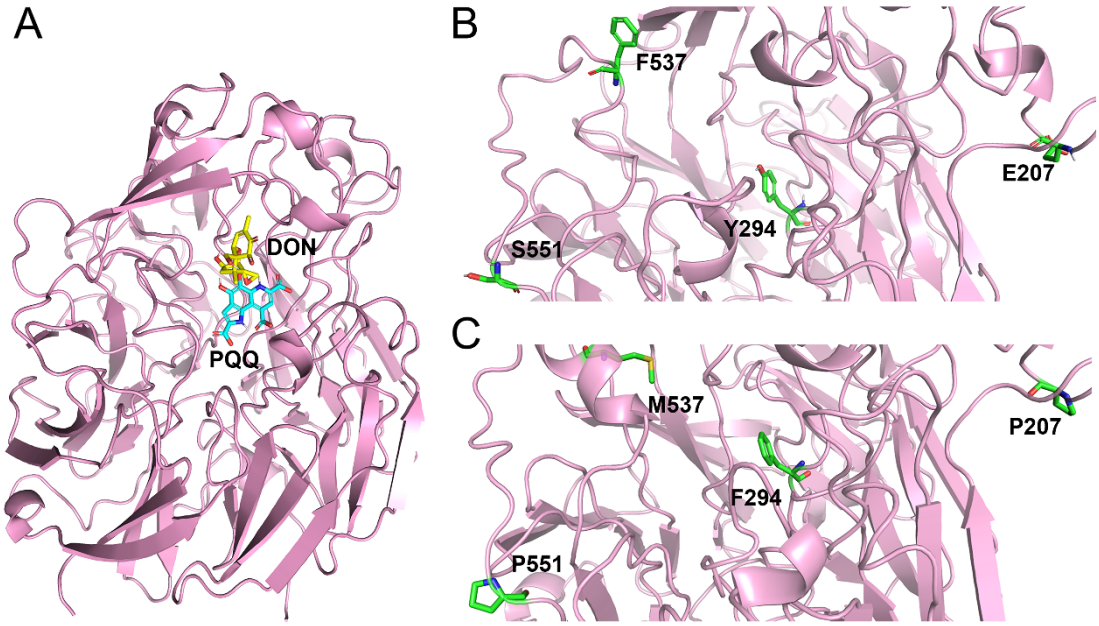

Figure 5. Structural analysis of the mechanism of increased thermostability. (A) Complex model of WT (DADH-V2/DON/PQQ), DON was shown as a wheat stick model, PQQ was shown as a cyan stick model. The four mutation sites F537, E207, S551, and Y294 (B) were replaced with M537, P207, P551, and F294 (C), respectively. Residues were displayed as green stick models.

MD simulations of WT and M3 were conducted to investigate the dynamic changes at 330 K for 50 ns. Root-mean-square deviation (RMSD) was presented as a crucial indicator for gauging the thermal fluctuation in enzyme conformation. The structural rigidity of the enzyme was positively correlated with the thermostability and negatively correlated with the fluctuation of RMSD values (Chen et al., 2024). As seen in Figure 6A, the fluctuation of RMSD values within 50 ns was smaller for variant M3 than that of the WT, indicating increased structural rigidity and stability of M3. The radius of gyration (Rg) also responds to the conformational stability of the enzyme and the lower the Rg value presented a more stable enzyme structure

(Chi et al., 2022). M3 had a lower average Rg value than WT, indicating a more compacted protein structure of M3 than that of WT (Figure 6B). The solvent accessible surface area (SASA) refers to the portion of a protein's surface that is available for interaction with solvent molecules. Briefly, the decline in SASA values during the simulation demonstrated that the protein adopted a more compact conformation, which in turn contributed to an improvement in its stability (Li et al., 2022). The average SASA value for WT was 202.08 Å², while the value for M3 dropped to 200.26 Å², demonstrating a reduction in the contact area between M3 and the solvent (Figure 6C). The root-mean-square fluctuations (RMSF) represented the fluctuation of amino acid residues in a protein (Wang et al., 2020). Smaller RMSF values suggested lower residue fluctuations and improved stability. The RMSF values of most regions of M3 were lower than those of WT, indicating that variant M3 had a more rigid and stable structure (Figure 6D). To sum up, as demonstrated by the RMSD, Rg, SASA, and RMSF analyses, M3 developed a more condensed and stable structure after 50 ns of molecular dynamics simulations at 330 K.

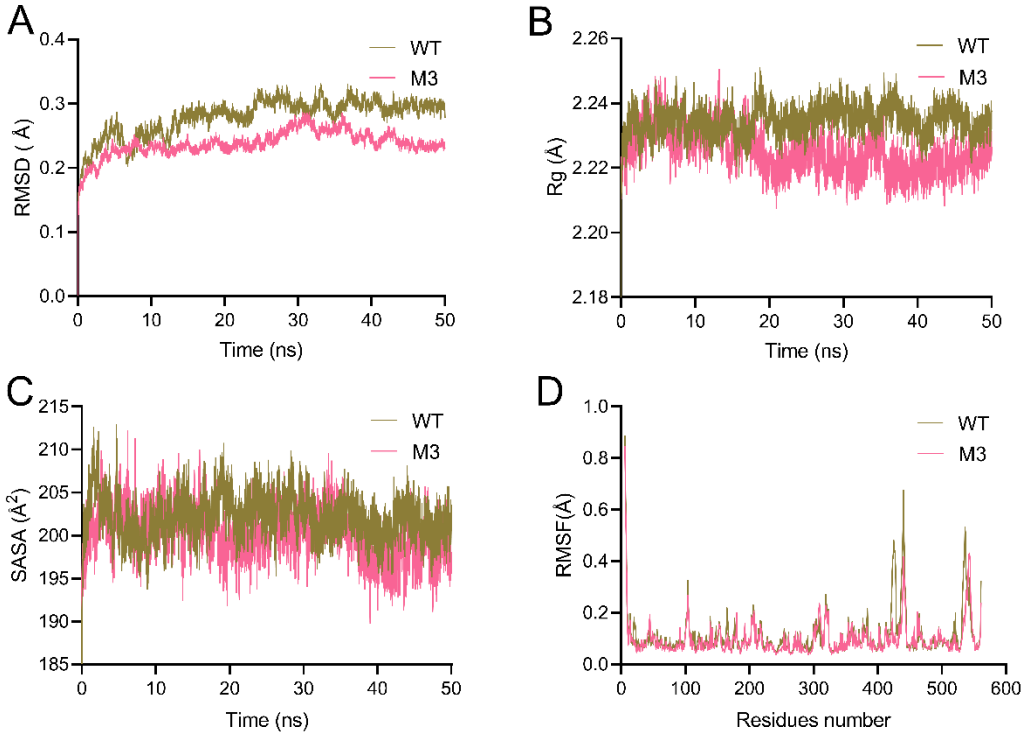

Figure 6. MD simulations revealed RMSD (A), Rg (B), SASA (C) and RMSF (D) results for WT and M3.

The thermostability of enzymes could also be improved by increasing the number of hydrogen bonds, since the novel bonds likely stiffen the protein scaffold (Shen et al., 2023). Compared to WT, the number of hydrogen bonds in M3 significantly increased, indicating a more stable structure that contributed to improved thermostability (Figure S5). Notably, residue F537 formed one hydrogen bond with A534 in WT, while residue M537 in M3 not only formed one hydrogen bond with A534 but also formed two hydrogen bonds with S541 (Figure S6). These results were consistent with the reduced fluctuations in RMSD values of M3 (Figure 6A). Additionally, principal component analysis (PCA) was performed to analyze the free energy of the WT and M3. Cluster analysis of the distribution of free energies revealed a decrease in the overall intensity of the red region in M3 compared to WT, whereas the low free energy region was enlarged (Figure 7A, B),

indicating increased conformational stability (Wang et al., 2023). The thermal unfolding and refolding behavior of an enzyme is profoundly impacted by its net surface charge (Wu et al., 2023). To further explore the mechanism of the improved thermostability of M3, the symmetry of the electrostatic potential on the surface of the protein has also been studied. A larger symmetric positive potential might lead to increased thermostability (Chi et al., 2022; Jiang et al., 2021). The electrostatic potential of WT indicated that S551 was positioned in the negative potential region (Figure 7C), and were inconsistent with the surrounding potential distribution, which was not favorable for enzyme stability. The amino acid residues M537, P207, F294, and P551 of M3 were nearly identical to the surrounding potential distribution, which was neutral at the P551 sites (Figure 7D). Moreover, a higher net surface charge acts as a safeguard against dehydrogenase aggregation, promoting the enzyme's reversible refolding process. The findings demonstrated that an elevation in the net surface charge contributed to the enhanced thermal stability of the mutant. These findings provided potential perspectives for clarifying the mechanism underlying the enhanced thermal stability of dehydrogenases.

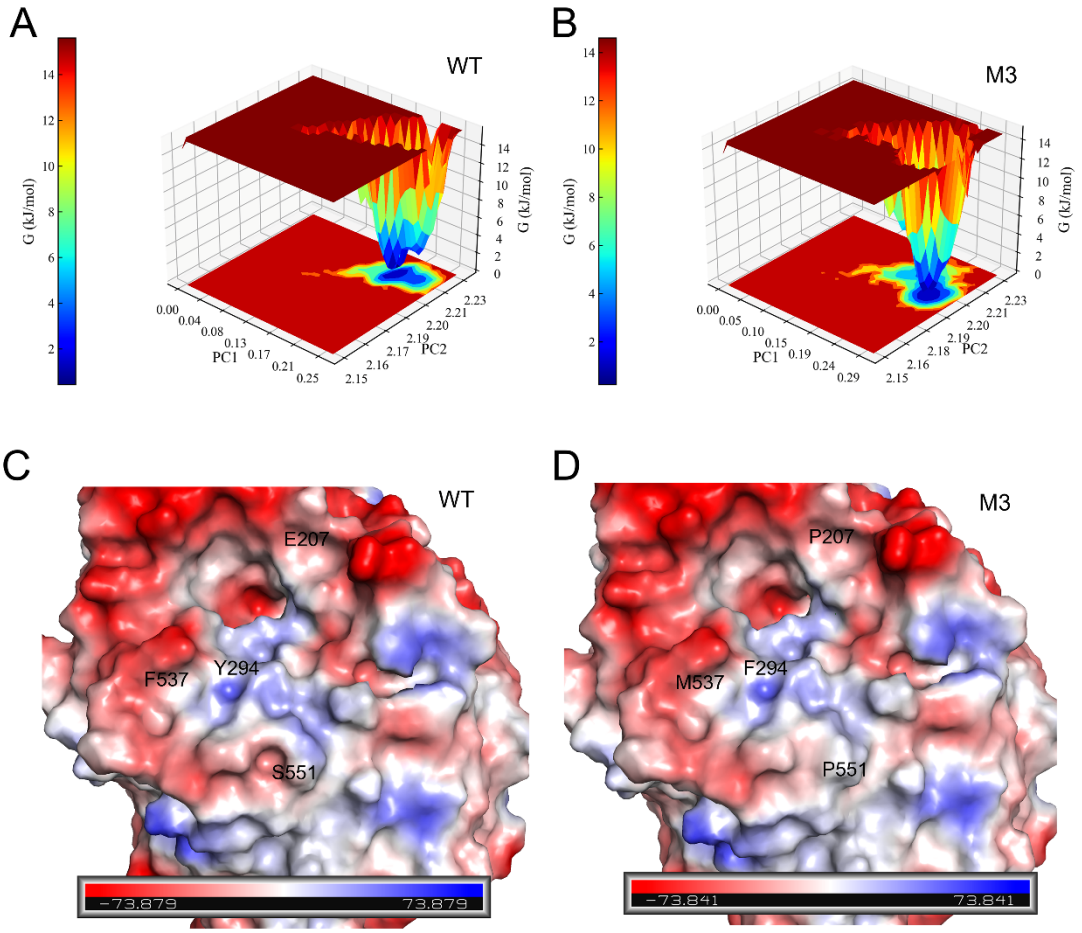

Figure 7. Free energy landscape of WT (A) and M3 (B) at 330 K. Dark blue indicated the lower relative free energy. Variation of electrostatic potential distribution on the surface of WT (C) and M3 (D). Positive, negative, and neutral values of electrostatic potentials were indicated by shades of blue, red, and white color respectively.

4. Conclusions

Deoxynivalenol (DON), a ubiquitous mycotoxin, was a major contaminant of cereals and cereal products. It was widespread in the food chain and represents a significant threat to the health of both human and animal. DADH, a novel quinone-dependent alcohol dehydrogenase, could oxidize DON into less-toxic

3-keto-DON. In our previous study, we enhanced the catalytic activity and substrate specificity of DADH and named the mutant DADH-V2. To further improve the practical application potential of DADH-V2, the drawback of its poor thermal stability needs to be addressed. This research utilized computation-aided design, combining ASRs strategy and structural analysis, to discover potential hotspots related to thermostability. By employing targeted mutagenesis and combinatorial mutagenesis, we succeeded in obtaining a mutant M3 with enhanced thermostability. The mutant M3 showed a notable 8.93-fold enhancement in $t_{1/2}$ at 55℃ along with 4.6℃ elevation in T_m, and was able to equilibrate the enzyme activity without a significant decrease. As evidenced by MD and structural analyses, the enhanced thermostability of mutant M3 primarily stemmed from its augmented structural rigidity and optimized electrostatic potential. Given that the results of this study could facilitate the utilization of M3 in high-temperature situations, this would cause its industrial applications to expand. Our investigation provides a practical approach to optimize DADH as an efficient and environmentally friendly detoxification catalyst for the food and feed industries.

Declaration of competing interest

The authors declare no competing financial interests.

Acknowledgments

This work was funded by the Jiangsu Provincial Frontier Technology Research and Development Program (BF2024073), the National Natural Science Foundation of China (32272267), and Fundamental Research Funds for the Central Universities (KYCYXT2023003).

Supplemental material

Supplemental material includes primers used in this paper, phylogenetic tree, $\Delta\Delta G$ values measured by CUPSAT, dynamic analysis, hydrophobicity and average flexibility analysis, number of hydrogen bonds.

References

Brennan, C. K., Livada, J., Martinez, C. A., Lewis, R. D. (2024). Ancestral sequence reconstruction meets machine learning: ene reductase thermostabilization yields enzymes with improved reactivity profiles. ACS Catal. 14(23), 17893-17900. https://doi.org/10.1021/acscatal.4c03738.

Cai, X., Jiang, H., Zhang, T., Jiang, B., Mu, W., Miao, M. (2018). Thermostability and specific-activity enhancement of an arginine deiminase from *Enterococcus faecalis* SK23.001 via semirational design for L-citrulline production. J. Agric. Food Chem. 66(33), 8841-8850. https://doi.org/10.1021/acs.jafc.8b02858.

Carere, J., Hassan, Y. I., Lepp, D., Zhou, T. (2018a). The enzymatic detoxification of the mycotoxin deoxynivalenol: Identification of DepA from the DON epimerization pathway. Microb. Biotechnol. 11(6), 1106-1111. https://doi.org/10.1111/1751-7915.12874.

Carere, J., Hassan, Y. I., Lepp, D., Zhou, T. (2018b). The identification of DepB: an enzyme responsible for the final detoxification step in the deoxynivalenol epimerization pathway in *Devosia* mutans 17-2-E-8. Front. Microbiol. 9, 1573. https://doi.org/10.3389/fmicb.2018.01573.

Chen, C., Guan, B.-H., Geng, Q., Zheng, Y.-C., Chen, Q., Pan, J., Xu, J.-H. (2023). Enhanced thermostability of *Candida* ketoreductase by computation-based cross-regional combinatorial mutagenesis. ACS Catal. 13(11), 7407-7416. https://doi.org/10.1021/acscatal.3c00503.

Chen, L., Yu, K., Ma, A., Zhu, W., Wang, H., Tang, X., Li, J. (2024). Enhanced thermostability of nattokinase by computation-based rational redesign of flexible regions. J. Agric. Food Chem. 72(25), 14241-14254. https://doi.org/10.1021/acs.jafc.4c02335.

Chen, X., Dou, Z., Luo, T., Sun, Z., Ma, H., Xu, G., Ni, Y. (2022). Directed reconstruction of a novel ancestral alcohol dehydrogenase featuring shifted pH-profile, enhanced thermostability and expanded substrate spectrum. Bioresource Technol. 363, 127886. https://doi.org/10.1016/j.biortech.2022.127886.

Chi, H., Wang, Y., Xia, B., Zhou, Y., Lu, Z., Lu, F., Zhu, P. (2022). Enhanced thermostability and molecular insights for L-asparaginase from *Bacillus licheniformis* via structure- and computation-based rational design. J. Agric. Food Chem. 70(45), 14499-14509. https://doi.org/10.1021/acs.jafc.2c05712.

Deng, Y., You, L., Wang, X., Wu, W., Kuca, K., Wu, Q., Wei, W. (2023). Deoxynivalenol: emerging toxic mechanisms and control strategies, current and future perspectives. J. Agric. Food Chem. 71(29), 10901-10915. https://doi.org/10.1021/acs.jafc.3c02020.

Fang, H., Zhang, C., Sun, A., Man, C., Zhang, Q., Kuang, Y., Shao, T. (2022). Effect of reactive chemical species on the degradation of deoxynivalenol, 3-acetyldeoxynivalenol, and 15-acetyldeoxynivalenol in low-temperature plasmas. ACS Food Sci. Technol. 2(3), 558-567. https://doi.org/10.1021/acsfoodscitech.1c00445.

Gumulya, Y., Baek, J., Wun, S., Thomson, R., Harris, K., Hunter, D., Wu, X. (2018). Engineering highly functional thermostable proteins using ancestral sequence reconstruction. Nat. Catal. 1, 878–888. https://doi.org/10.1038/s41929-018-0159-5.

Gumulya, Y., Gillam, E. M., 2017. Exploring the past and the future of protein evolution with ancestral sequence reconstruction: the 'retro' approach to protein engineering. Biochem. J. 474(1), 1-19. https://doi.org/10.1042/BCJ20160507.

Guo, C., Wen, J., Sun, Y., Liang, G., Wang, Z., Pan, L., Chen, Q. (2024). Pyrroloquinoline quinone production defines the ability of *Devosia* species to degrade deoxynivalenol. Food Funct. 15(11), 6134-6146. https://doi.org/10.1039/D4FO00024B.

Hasan, W. A. N. B. W., Nezhad, N. G., Yaacob, M. A., Salleh, A. B., Rahman, R. N. Z. R. A., Leow, T. C. (2024). Shifting the pH profiles of *Staphylococcus epidermidis* lipase (SEL) and *Staphylococcus hyicus* lipase (SHL) through generating chimeric lipases by DNA shuffling strategy. World J. Microb. Biot. 40(4), 106. https://doi.org/10.1007/s11274-024-03927-x.

He, W.-J., Shi, M.-M., Yang, P., Huang, T., Zhao, Y., Wu, A.-B., Liao, Y.-C. (2020). A quinone-dependent dehydrogenase and two NADPH-dependent aldo/keto reductases detoxify deoxynivalenol in wheat via epimerization in a *Devosia* strain. Food Chem. 321, 126703. https://doi.org/10.1016/j.foodchem.2020.126703.

He, W.-J., Zhang, L., Yi, S.-Y., Tang, X.-L., Yuan, Q.-S., Guo, M.-W., Liao, Y.-C. (2017). An aldo-keto reductase is responsible for *Fusarium* toxin-degrading activity in a soil *Sphingomonas* strain. Sci. Rep. 7(1), 9549. https://doi.org/10.1038/s41598-017-08799-w.

Jiang, X., Wang, Y., Wang, Y., Huang, H., Bai, Y., Su, X., Zhang, J., Yao, B., Tu, T., Luo, H. (2021). Exploiting the activity-stability trade-off of glucose oxidase from *Aspergillus niger* using a simple approach to calculate thermostability of mutants. Food Chem. 342, 128270. https://doi.org/10.1016/j.foodchem.2020.128270.

Khatibi, P. A., Montanti, J., Nghiem, N. P., Hicks, K. B., Berger, G., Brooks, W. S., Schmale, D. G. (2011). Conversion of deoxynivalenol to 3-acetyldeoxynivalenol in barley-derived fuel ethanol co-products with yeast expressing trichothecene 3-O-acetyltransferases. Biotechnol. Biofuels 4(1), 26. https://doi.org/10.1186/1754-6834-4-26.

Li, D., Liang, G., Mu, P., Lin, J., Huang, J., Guo, C., Wu, J. (2023). Improvement of catalytic activity of sorbose dehydrogenase for deoxynivalenol degradation by rational design. Food Chem. 423, 136274. https://doi.org/10.1016/j.foodchem.2023.136274.

Li, T., Cui, N., Fan, J., Liu, X., Guan, J., Zhang, W., Xu, Y. (2022). Engineering β-agarase Aga0917 from *Pseudoalteromonas fuliginea* YTW1-15-1 to Improve the Thermostability and Enzyme Activity. ACS Sustainable Chem. Eng. 10(47), 15437-15449. https://doi.org/10.1021/acssuschemeng.2c04531.

Ma, B., Niu, J., Zhu, H., Chi, H., Lu, Z., Lu, F., Zhu, P. (2024). Engineering substrate specificity of quinone-dependent dehydrogenases for efficient oxidation of deoxynivalenol to 3-keto-deoxynivalenol. Int. J. Biol. Macromol. 264, 130484. https://doi.org/10.1016/j.ijbiomac.2024.130484.

Nie, Y., Wang, S., Xu, Y., Luo, S., Zhao, Y.-L., Xiao, R., Szyperski, T. (2018). Enzyme engineering based on X-ray structures and kinetic profiling of substrate libraries: alcohol dehydrogenases for stereospecific synthesis of a broad range of chiral alcohols. Acs Catal. 8(6), 5145-5152. https://doi.org/10.1021/acscatal.8b00364.

Niu, J., Ma, B., Shen, J., Chi, H., Zhou, H., Lu, Z., Lu, F., Zhu, P. (2023). Structure-guided steric hindrance engineering of *Devosia* strain A6–243 quinone-dependent dehydrogenase to enhance its catalytic efficiency. J. Agric. Food Chem., 72(1), 549-558. https://doi.org/10.1021/acs.jafc.3c07179.

Niu, J., Yan, R., Zhou, H., Ma, B., Lu, Z., Meng, F., Zhu, P. (2024). Self-cascade deoxynivalenol detoxification by an artificial enzyme with bifunctions of dehydrogenase and aldo/keto reductase from genome mining. Int. J. Biol. Macromol. 261, 129512. https://doi.org/10.1016/j.ijbiomac.2024.129512.

Qin, X., Zhang, J., Liu, Y., Guo, Y., Tang, Y., Zhang, Q., Zhao, L. (2022). A quinoprotein dehydrogenase from *Pelagibacterium halotolerans* ANSP101 oxidizes deoxynivalenol to 3-keto-deoxynivalenol. Food Control 136, 108834. https://doi.org/10.1016/j.foodcont.2022.108834.

Randall, R., Radford, C., Roof, K., Natarajan, D., Gaucher, E. (2016). An experimental phylogeny to benchmark ancestral sequence reconstruction. Nat. Commun. 7, 12847. https://doi.org/10.1038/ncomms12847.

Schmied, A., Marske, L., Berger, M., Kujath, P., Weber, T., Kolossa-Gehring, M. (2023). Human biomonitoring of deoxynivalenol (DON)-assessment of the exposure of young German adults from 1996-2021. Int. J. Hyg. Envir. Heal. 252, 114198. https://doi.org/10.1016/j.ijheh.2023.114198.

Schupfner, M., Straub, K., Busch, F., Merkl, R., Sterner, R. (2020). Analysis of allosteric communication in a multienzyme complex by ancestral sequence reconstruction. P. Nat. A. Sci. 117(1), 346-354. https://doi.org/10.1073/pnas.1912132117.

Shen, W., Dalby, P. A., Guo, Z., Li, W., Zhu, C., Fan, D. (2023). Residue effect-guided design: engineering of *S. Solfataricus* β-glycosidase to enhance its thermostability and bioproduction of ginsenoside compound K. J. Agric. Food Chem. 71(44), 16669-16680. https://doi.org/10.1021/acs.jafc.3c04575.

Spence, M. A., Kaczmarski, J. A., Saunders, J. W., Jackson, C. J. (2021). Ancestral sequence reconstruction for protein engineers. Curr. Opin. Struc. Biol. 69, 131-141. https://doi.org/10.1016/j.sbi.2021.04.001.

Sumarah, M. W. (2022). The deoxynivalenol challenge. J. Agric. Food Chem. 70(31), 9619-9624. https://doi.org/10.1021/acs.jafc.2c03690.

Tamura, K., Stecher, G., Kumar, S. (2021). MEGA11: Molecular Evolutionary Genetics Analysis Version 11. Mol. Biol. Evol. , 38 (7), 3022−3027. https://doi.org/10.1093/molbev/msab120.

Thomson, R. E., Carrera-Pacheco, S. E., Gillam, E. M. (2022). Engineering functional thermostable proteins using ancestral sequence reconstruction. J. Biol. Chem. 298(10), 102435. https://doi.org/10.1016/j.jbc.2022.102435.

Tian, Y., Tan, Y., Liu, N., Yan, Z., Liao, Y., Chen, J., Wu, A. (2016). Detoxification of deoxynivalenol via glycosylation represents novel insights on antagonistic activities of *Trichoderma* when confronted with *Fusarium* graminearum. Toxins 8(11), 335. https://doi.org/10.3390/toxins8110335.

Tian, Y., Zhang, D., Cai, P., Lin, H., Ying, H., Hu, Q.-N., Wu, A. (2022). Elimination of *Fusarium* mycotoxin deoxynivalenol (DON) via microbial and enzymatic strategies: Current status and future perspectives. Trends Food Sci. Tech. 124, 96-107. https://doi.org/10.1016/j.tifs.2022.04.002.

Truongvan, N., Jang, S.-H., Lee, C. (2016). Flexibility and stability trade-off in active site of cold-adapted *Pseudomonas mandelii* Esterase EstK. Biochemistry 55(25), 3542-3549. https://doi.org/10.1021/acs.biochem.6b00177.

Tu, Y., Liu, S., Cai, P., Shan, T. (2023). Global distribution, toxicity to humans and animals, biodegradation, and nutritional mitigation of deoxynivalenol: A review. Compr. Rev. Food Sci. F. 22(5), 3951-3983. https://doi.org/10.1111/1541-4337.13203.

Wang, G., Wang, Y., Ji, F., Xu, L., Yu, M., Shi, J., Xu, J. (2019). Biodegradation of deoxynivalenol and its derivatives by *Devosia* insulae A16. Food Chemistry 276, 436-442. https://doi.org/10.1016/j.foodchem.2018.10.011.

Wang, L.-Y., Tang, H., Zhao, J.-Q., Wang, M.-N., Xue, Y.-P., Zheng, Y.-G. (2023). Correlation analysis of key residue sites between computational-aided design thermostability D-amino acid oxidase and ancestral enzymes. J. Agric. Food Chem. 71(50), 20177-20186. https://doi.org/10.1021/acs.jafc.3c06865.

Wang, R., Wang, S., Xu, Y., Yu, X. (2020). Enhancing the thermostability of *Rhizopus chinensis* lipase by rational design and MD simulations. Int. J. Biol. Macromol. 160, 1189-1200. https://doi.org/10.1016/j.ijbiomac.2020.05.243.

Wang, Z.-K., Feng, D.-T., Su, C., Li, H., Rao, Z.-M., Rao, Y.-J., Gong, J.-S. (2024). Designing ASSMD strategy for exploring and engineering extreme thermophilic ancestral nitrilase for nitriles biocatalysis. Acs Catal. 14(18), https://doi.org/10.1021/acscatal.4c03851.

Wu, Q., Zhang, C., Dong, W., Lu, H., Yang, Y., Li, W., Li, X. (2023). Simultaneously enhanced thermostability and catalytic activity of xylanase from *Streptomyces rameus* L2001 by rigidifying flexible regions in loop regions of the N-terminus. J. Agric. Food Chem. 71(34), 12785-12796. https://doi.org/10.1021/acs.jafc.3c03871.

Yang, C., Hu, G., Xiang, X., Wu, D., Wang, B., Wang, J., Geng, F. (2023). Translucency mechanism of heat-induced pigeon egg white gel. Int. J. Biol. Macromol. 253, 126909. https://doi.org/10.1016/j.ijbiomac.2023.126909.

Yang, H., Yan, R., Li, Y., Lu, Z., Bie, X., Zhao, H., Chen, M. (2022). Structure–function analysis of a quinone-dependent dehydrogenase capable of deoxynivalenol detoxification. J. Agric. Food Chem. 70(22), 6764-6774. https://doi.org/10.1021/jacsau.3c00696.

Yang, J., Liang, K., Ke, H., Zhang, Y., Meng, Q., Gao, L., Xiao, J. (2024). Enzymatic degradation of deoxynivalenol with the engineered detoxification enzyme Fhb7. JACS Au 4(2), 619-634. https://doi.org/10.1021/jacsau.3c00696.

Yao, F., Du, Y., Tian, S., Chang, G., Zhang, Y., Cai, C., Zhou, T. (2024). Strategies for deoxynivalenol (DON) degradation by microbes from organic fertilizers and influence of the bacterial diversity after DON treatment. Int. Biodeter. Biodegr. 187, 105725. https://doi.org/10.1016/j.ibiod.2023.105725.

Zhang, C., Gao, W., Song, Z., Dong, M., Lin, H., Zhu, G., Lian, M., Xiao, Y., Lu, F., Wang, F., Liu, Y. (2024). Computation-aided phylogeny-oriented engineering of *β*-xylosidase: modification of “Blades” to enhance stability and activity for the bioconversion of hemicellulose to produce xylose. J. Agric. Food Chem. 72(5), 2678-2688. https://doi.org/10.1021/acs.jafc.3c08518.

Zhang, H., Zhang, H., Qin, X., Wang, X., Wang, Y., Bin, Y., Luo, H. (2021). Biodegradation of deoxynivalenol by *Nocardioides* sp. ZHH-013: 3-keto-deoxynivalenol and 3-*epi*-deoxynivalenol as intermediate products. Front. Microbiol. 12, 658421. https://doi.org/10.3389/fmicb.2021.658421.

Zhang, Y., Ouyang, B., Zhang, W., Guang, C., Xu, W., Mu, W. (2024). Deoxynivalenol: occurrence, toxicity, and degradation. Food Control 155, 110027. https://doi.org/10.1016/j.foodcont.2023.110027.